SAND2017-3683C

Finite-Difference Algorithm for 3D Orthorhombic Elastic Wave Propagation

Leiph A. Preston, Richard P. Jensen, and **David F. Aldridge**
Geophysics Department, Sandia National Laboratories, Albuquerque, New Mexico

Intro to Orthorhombo

Many geophysicists concur that an ***orthorhombic*** elastic medium, characterized by three mutually orthogonal symmetry planes, constitutes a realistic representation of seismic anisotropy in shallow crustal rocks. This symmetry condition typically arises via a dense system of vertically-aligned microfractures superimposed on a finely-layered horizontal geology:

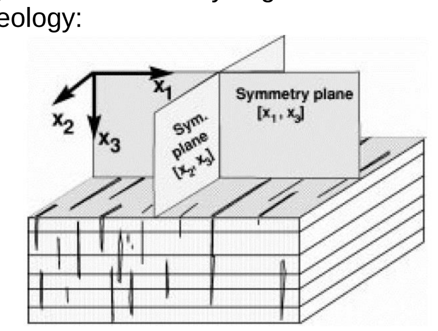

FIG. 1. An orthorhombic model caused by parallel vertical cracks embedded in a medium composed of thin horizontal layers. Orthorhombic media have three mutually orthogonal planes of mirror symmetry.

From Tsvankin, 1997, *Geophysics*.

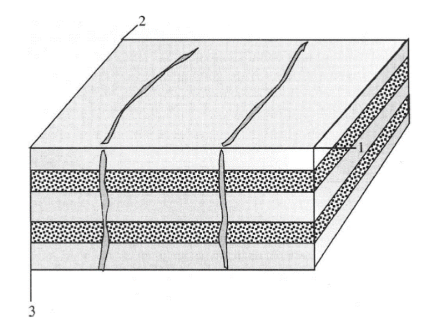

FIG. 1. Schematic diagram of long vertical fractures aligned in the 2,3-plane embedded in a TI medium with a vertical symmetry axis.

From Schoenberg and Helbig, 1997, *Geophysics*.

However, various geological deformation processes will rotate the symmetry planes away from alignment with the global XYZ coordinate planes:

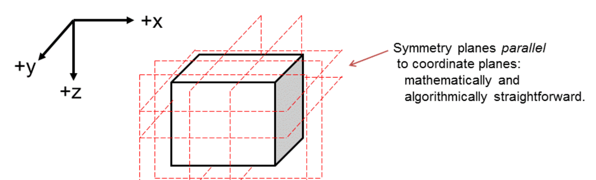

Present algorithmic assumption: 3 principal axes of orthorhombic elastic modulus tensor aligned with global XYZ coordinate axes.

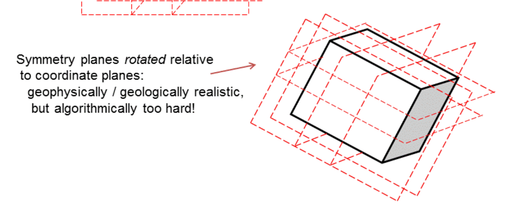

Rotated principal axes lead to significant algorithmic complications! Subject of future R&D.

Mathematically, the elastic stress-strain constitutive relations for an orthorhombic body contain nine independent moduli. In turn, these moduli can be determined by observing (or prescribing) nine independent P-wave and S-wave phase speeds along different directions (Brown, 1989):

6 P-Wave Speeds / Directions:

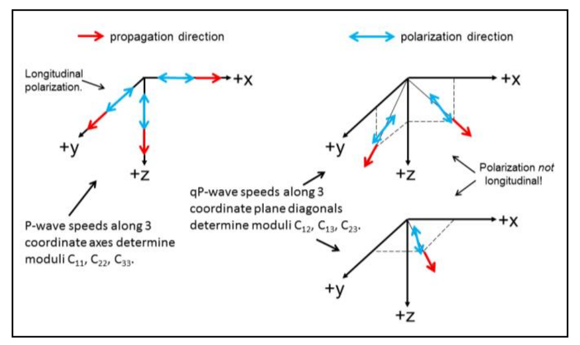

6 S-Wave Speeds / Directions:

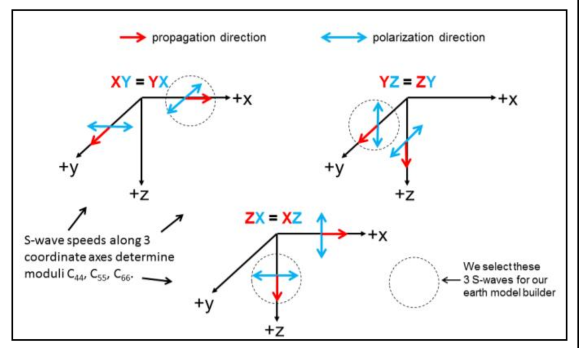

Standard TI and VF+TI Models
(after Schoenberg and Helbig, 1997)

The Wavespeeds

	VTI	VF+TI	ISO
$n=e_1$, $p=e_1$:	3500	3320	3500
$n=e_2$, $p=e_2$:	3500	3472	3500
$n=e_3$, $p=e_3$:	2711	2697	3500
$n=e_1$, $p=e_2$:	1917	1635	1565
$n=e_2$, $p=e_3$:	1565	1565	1565
$n=e_3$, $p=e_1$:	1565	1400	1565
$n=n_{12}$, $p \perp e_3$:	3500	3264	3500
$n=n_{23}$, $p \perp e_1$:	3023	3001	3500
$n=n_{31}$, $p \perp e_2$:	3023	2845	3500

The density-normalized modulus tensor (m^2/s^2)

$$A_{VF}=\begin{pmatrix} 9 & 3.6 & 2.25 & 0 & 0 & 0 \\ 3.6 & 9.84 & 2.4 & 0 & 0 & 0 \\ 2.25 & 2.4 & 5.9375 & 0 & 0 & 0 \\ 0 & 0 & 0 & 2 & 0 & 0 \\ 0 & 0 & 0 & 0 & 1.6 & 0 \\ 0 & 0 & 0 & 0 & 0 & 2.182 \end{pmatrix}$$

Mathematics!

Initial modeling utilizes the "standard model" of a VF+TI (vertical fractures + transverse isotropic) elastic model of Schoenberg and Helbig (1997), plus its TI and isotropic counterparts.

The anisotropic elastic ***velocity-stress system***, a set of 9 coupled, first-order, linear, inhomogeneous PDEs forms the mathematical basis for our explicit time-domain finite-difference (FD) numerical algorithm. All partial derivatives are discretized with centered and staggered FD operators that are 2nd-order in time and 4th-order in space:

Governing PDE System: Anisotropic Elastic Velocity-Stress System

$$\rho \frac{\partial v_i}{\partial t} - \frac{\partial \sigma_{ij}}{\partial x_j} = f_i + \frac{\partial m^a_{ij}}{\partial x_j} \qquad \text{3 equations of motion}$$

$$\frac{\partial \sigma_{ij}}{\partial t} - c_{ijkl}\frac{\partial v_k}{\partial x_l} = \frac{\partial m^s_{ij}}{\partial t} \qquad \text{6 stress/strain constitutive relations}$$

Nine, coupled, first-order, linear, non-homogeneous partial differential equations.

Wavefield variables: $v_i(\mathbf{x},t)$ - velocity vector; $\sigma_{ij}(\mathbf{x},t)$ - stress tensor

Earth model parameters: $\rho(\mathbf{x})$ - mass density; $c_{ijkl}(\mathbf{x})$ – modulus tensor ($c_{ijkl} = c_{jikl} = c_{ijlk} = c_{klij}$)

Body sources: $f_i(\mathbf{x},t)$ - force vector; $m_{ij}(\mathbf{x},t)$ - moment tensor

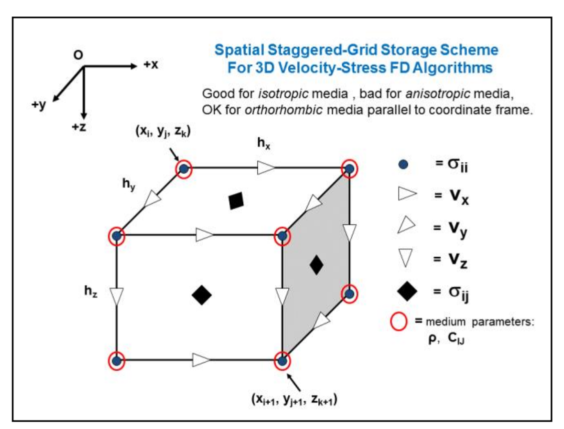

Propagating Orthorhombic Wavefronts *and* CPML ABC Performance

Explosion source ●

Double-halfspace model

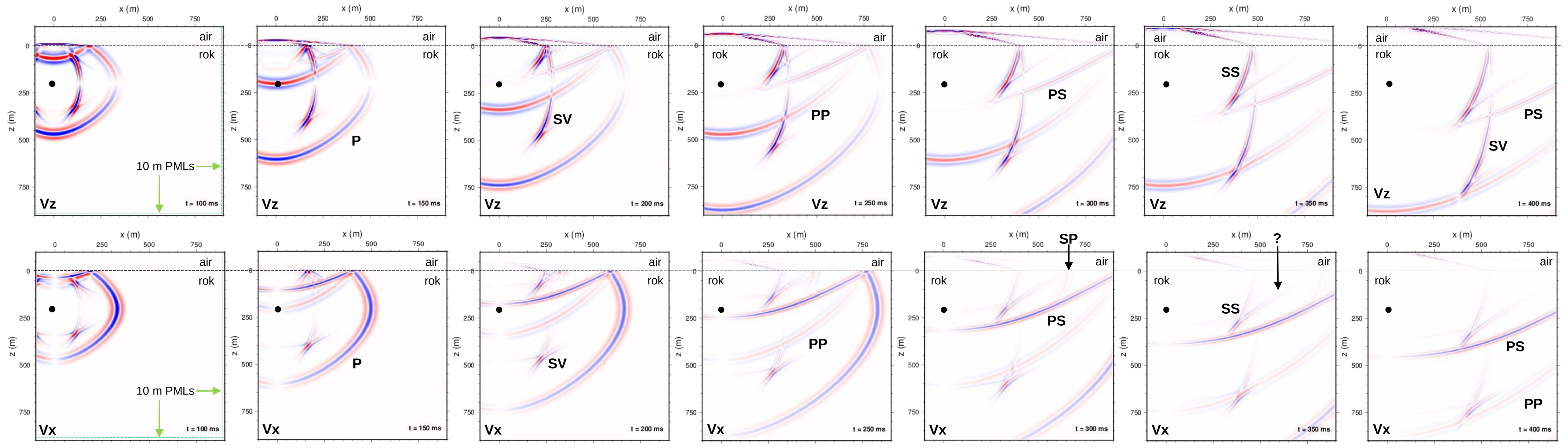

Note:

1) Air waves (~350 m/s) generated by conventional underground explosion.

2) SV-waves generated by conventional explosion source.

3) Nodal lines in source radiation pattern.

4) Surface reflected and converted modes.

5) SV triplications.

6) Surface head wave?

7) And

P- and S-wavefronts cleanly exit edges and corners of computational grid *without* generating any visible reflected or diffracted energy!

Explosion Source Wavefronts

Columns: media types (ISO = isotropic, TI = transverse isotopic, ORTO = orthorhombic)
Rows: wavefield variables (Vx, Vz = particle velocities, P = pressure, Wy = particle rotation rate)

Double-Halfspace Model: Air / Rock

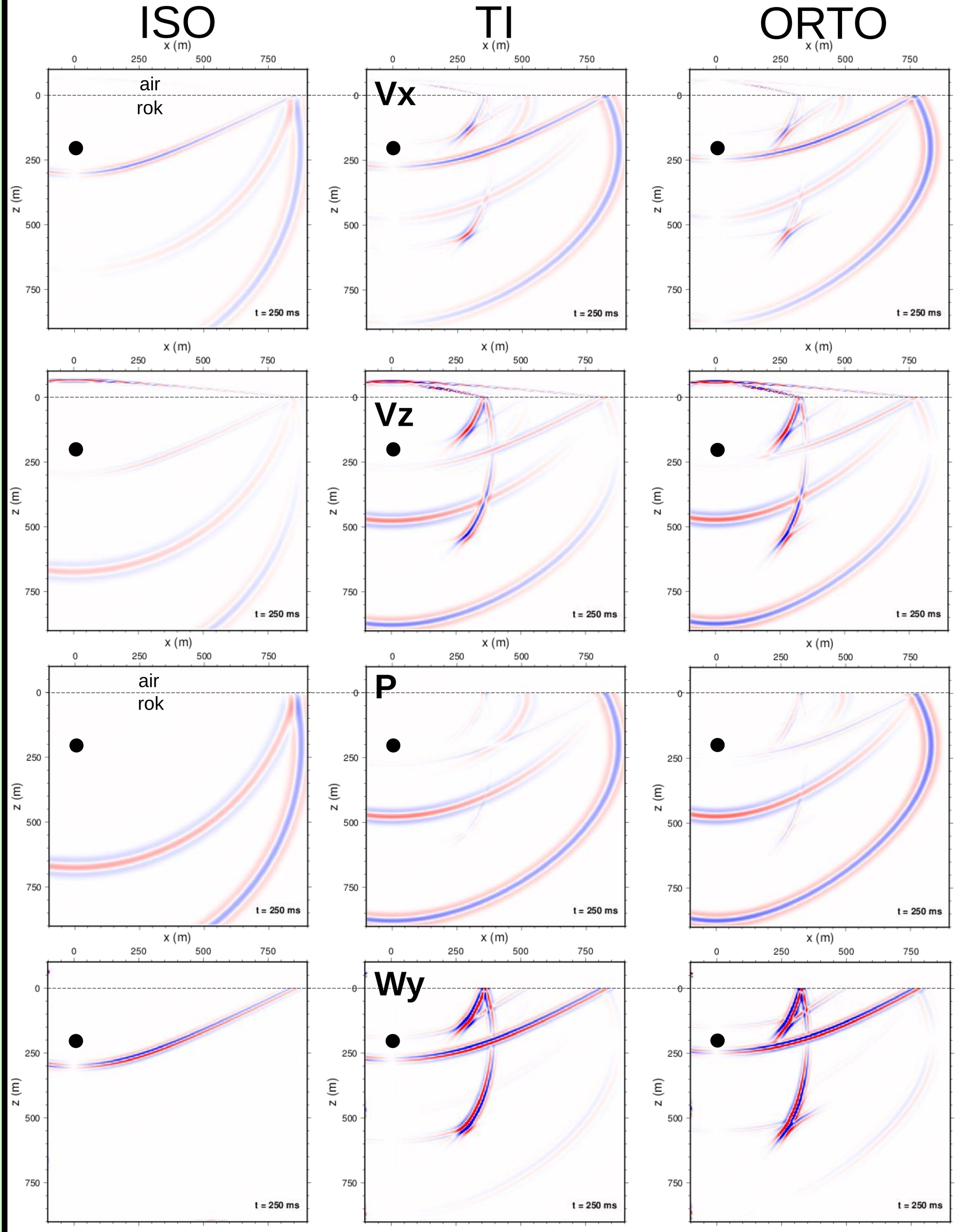

Explosion source generates SV waves in TI and ORTO

Note SV triplications

Surface reflected and converted waves

Strong shear from explosion source in TI and ORTO

Stronger air wave generation by Vz compared to Vx

Non-circular pressure wavefronts, and weak S-wave pressure signal, in TI and ORTO

Weak P and strong SV rotation wavefronts in TI and ORTO

Surface P to S conversion generates rotation signal

Explicit Stress-Free Surface: Vac / Rock

No **air waves (obviously)!**

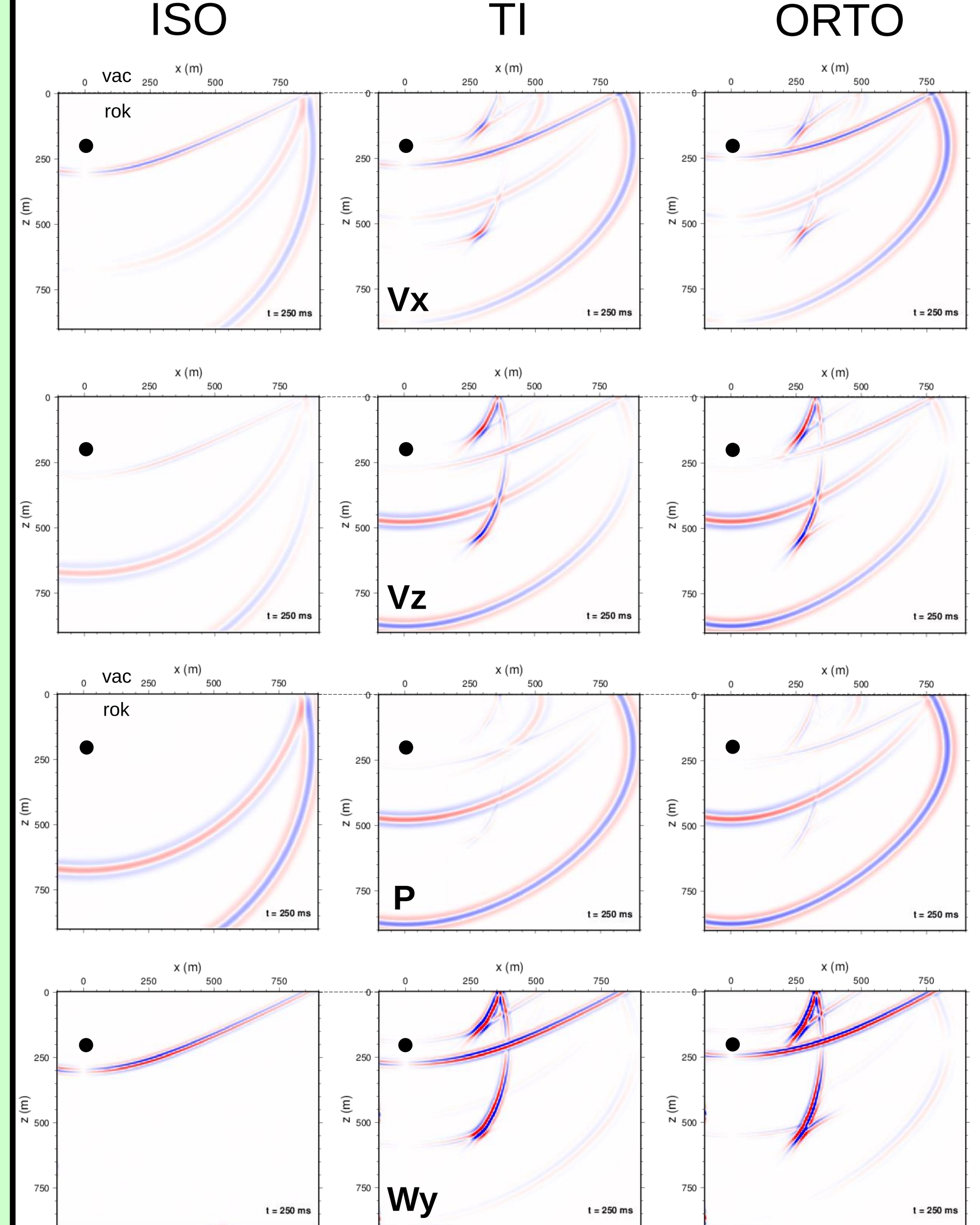

Explosion source generates SV waves in TI and ORTO

Note SV triplications

Surface reflected and converted waves

Strong shear from explosion source in TI and ORTO

Non-circular pressure wavefronts, and weak S-wave pressure signal, in TI and ORTO

Weak P and strong SV rotation wavefronts in TI and ORTO

Surface P to S conversion generates rotation signal

X-Direction Force (Fx) Source

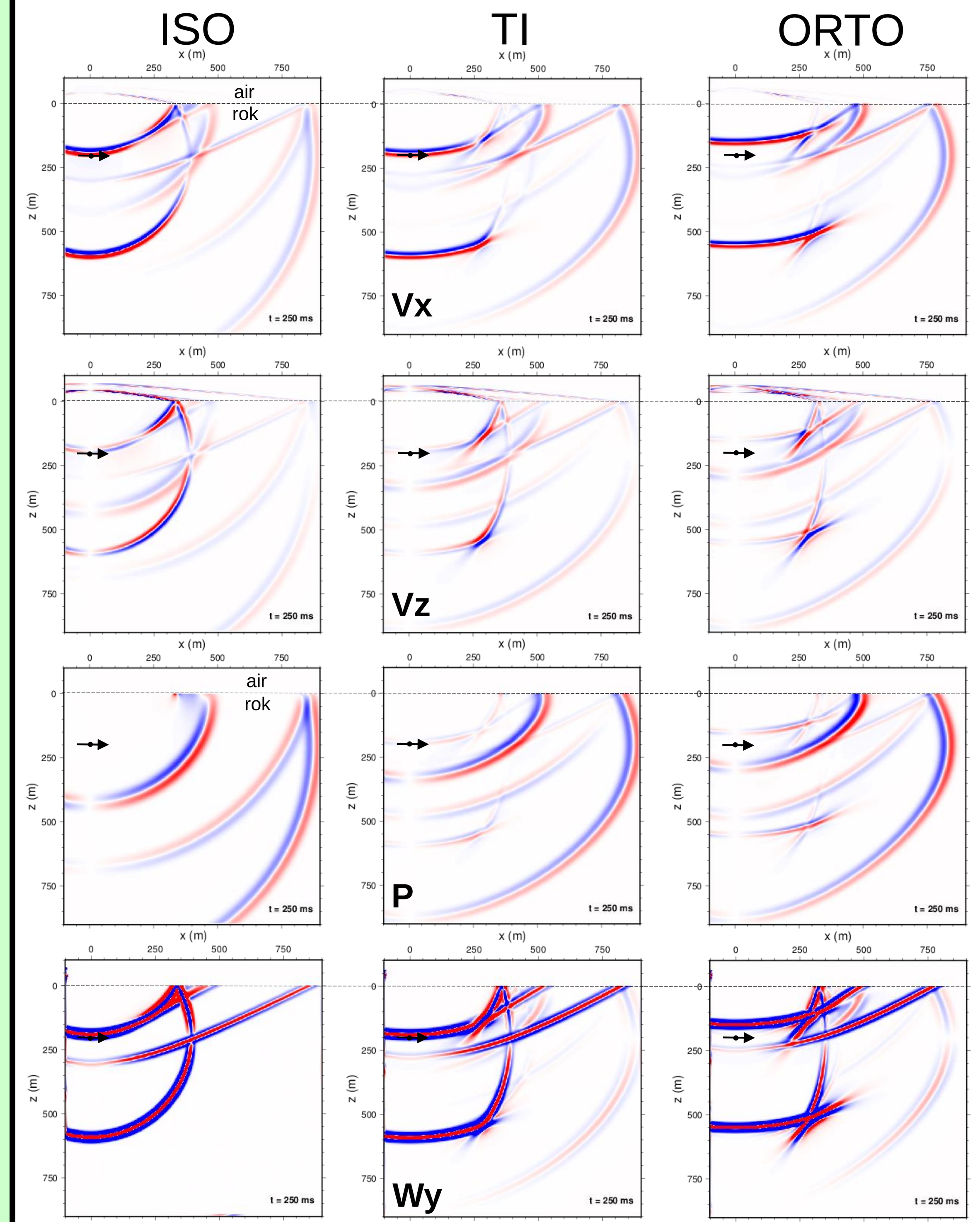

Outer wavefront: P-wave

Inner wavefront: SV wave

Surface reflections and conversions

Triplications in TI and ORTO SV wavefronts; none in ISO.

Strong air waves generated by Vz

Pressure wavefronts propagate with both P and S speeds in TI and ORTO media

SV waves generate strong rotation signal

Weak rotation wavefronts propagate with P speed in TI and ORTO media

Conclusions / Observations

Explicit time-domain finite-difference numerical algorithm demonstrates known anisotropic seismic phenomena of:

1) Complex wavefront shapes, 2) Pressure / rotation propagating with *both* P / S speeds,
3) Split (fast and slow) shear waves, 4) *Shear* waves from isotropic explosion.

5) Orthorhombic explicit stress-free surface compares well with double-halfspace (air over rock) model responses:
5.1) Smaller model implies smaller computational memory and faster execution, *but*
5.2) No air waves (e.g., infrasound) generated.

6) Air / rock or vacuum / rock (i.e., stress-free surface) is a *strong* generator of shear energy.

7) *Rotated* modulus tensor axes next R&D task!

Acknowledgements

Sandia National Laboratories is a multi-mission laboratory managed and operated by Sandia Corporation, a wholly-owned subsidiary of Lockheed Martin Corporation, for the US Department of Energy's National Nuclear Security Administration under contract DE-AC04-94AL85000. The present work is conducted under the auspices of the Source Physics Experiment (SPE) funded by the Office of Defense Nuclear Nonproliferation Research and Development (DNN R&D) of the NNSA.

References

Brown, R.J., 1989, Relationships between the velocities and the elastic constants of an anisotropic solid possessing orthorhombic symmetry: Research Report 1989-17, Consortium for Elastic Wave Exploration Seismology (CREWES), University of Calgary.
Jensen, R.P., Preston, L.A., and Aldridge, D.F., 2016, Finite-difference algorithm for 3D orthorhombic elastic wave propagation: American Geophysical Union Annual Fall Meeting, 12-16 December 2016, San Francisco, CA, USA.
Schoenberg, M., and Helbig, K., 1997, Orthorhombic media: modeling of elastic wave behavior in a vertically fractured earth: Geophysics, **62**, 1954-1974.
Tsvankin, I., 1997, Anisotropic parameters and P-wave velocity for orthorhombic media: Geophysics, **62**, 1292-1309.